

Studentská přehlídka II

SL6

X-RAY DIFFRACTION ON VERTICALLY MODULATED SUPERLATTICES

Petr Machovec

Faculty of Mathematics and Physics, Charles University, Ke Karlovu 5, 121 16 Praha 2
 machovec9@seznam.cz

Superlattice is a periodic structure of layers of two or more materials. Superlattices are being widely investigated for their unique electronic and magnetic properties. Recent advances in deposition methods have allowed the creation of complex superlattices with promising applications in solar cells, sensors, spintronics, and data storage. Deposition of superlattices requires very precise tuning of the deposition process. One of the challenges of creating high-quality superlattices is the precise control of the amount of deposited material. In our work, we present a new method for post-deposition calibration of the deposition process.

If the amount of material deposited for each layer is more or less than the exact amount needed for one layer, the resulting superlattice has vertical modulation. This means that the chemical composition of the superlattice has a period that is not equal to an integer number of monolayers. We can characterize this by a parameter called wavelength of modulation, which is the vertical period of chemical composition. shows the difference between ideal and modulated superlattice.

The x-ray diffraction on the modulated superlattice is calculated by the following process. First, the occupancies of each material for each layer are calculated from the wavelength of modulation. And then, the structure factor of the superlattice is calculated as a coherent sum of the structure factors of both materials weighted by the occupations in each layer.

Vertical modulation causes a systematic shift and splitting of superlattice maxima in 2θ scans. Additionally, it is possible to include lateral inhomogeneity of the layers into the simulation. This causes a broadening of the superlattice maxima. In Figure 2 we show simulation and measurement of 2θ scan of $2(\text{SrIrO}_3)/1(\text{SrTiO}_3)/1(\text{SrIrO}_3)/1(\text{SrTiO}_3)$ superlattice with the vertical modulation period equal to 1.025 of the superlattice period.

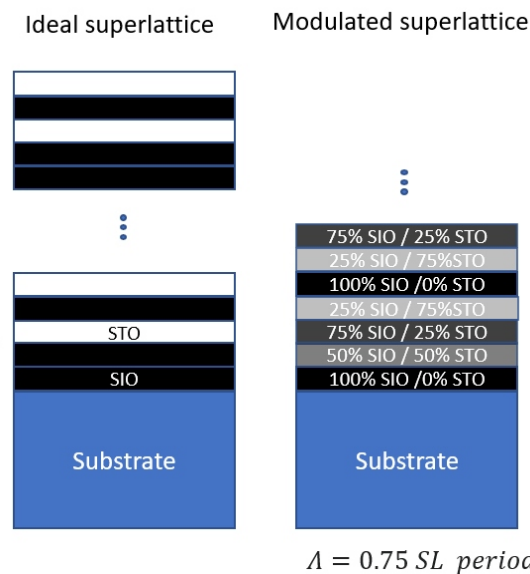


Figure 1. Schematically shown the difference between the ideal (left) and modulated (right) superlattice. The ideal superlattice is $2(\text{SrIrO}_3)/1(\text{SrTiO}_3)/1(\text{SrIrO}_3)/1(\text{SrTiO}_3)$. The modulation wavelength of the superlattice in the picture is 0.75 of the ideal superlattice period.

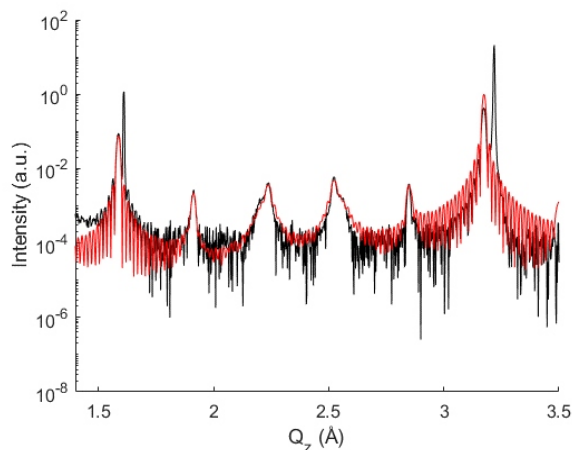


Figure 2: $2\theta/\theta$ scan of $2(\text{SrIrO}_3)/1(\text{SrTiO}_3)/1(\text{SrIrO}_3)/1(\text{SrTiO}_3)$ superlattice with modulation 1.025 of superlattice period. Measured data are plotted in black and simulation in red.



SL7

RAMAN SPECTROSCOPY OF FERROELECTRIC PHASE TRANSITIONS

P. Pazourek

Department of Condensed Matter Physics, Faculty of Science, Masaryk University, Kotlářská 2,
Brno, Czech Republic
petrpazourek@mail.muni.cz

The combination of topological insulators with ferroelectric properties allows to influence band structure of the surface states. This work inquires into Raman spectroscopy of ferroelectric phase transitions of chalcogenide compounds (SnTe, SnGeTe, PbGeTe, PbSnTe, and PbSnSe). By cooling below the critical temperature, crystal structure of these compounds changes from the rock-salt, i.e. two interpen-

etrating FCC lattices, to rhombohedral, and the compounds become Raman active. The Raman spectra were measured in the range from 300 K to 75 K, and by cooling below the critical temperature new phonons appeared in the spectra as well as phonons with temperature-dependent Raman shift.

SL8

THE REAL STRUCTURE OF γ -Fe PHASE OF ROLLED AISI 2205 DUPLEX STAINLESS STEEL AFTER SHOT PEENING

M. Rušin, J. Čapek, K. Trojan

Department of Solid State Engineering, Faculty of Nuclear Sciences and Physical Engineering,
Czech Technical University in Prague
rusinma3@cvut.cz

Duplex (stainless) steels are a family of grades that are used in areas such as automotive, aviation industry, civil engineering, and food storage. Two main phases are α -Fe and γ -Fe, mostly in a 1:1 ratio. Duplex steels exhibit better properties, such as corrosion resistance, compared to single-phase steels [1]. Post-processing, e.g., Shot Peening (SP), is used to further improve the final mechanical properties of the steel. The main purpose is to generate compressive residual stresses in the surface and subsurface layers of the peened material. As crack initiation and propagation are reduced in a compressively stressed zone, SP provides a considerable increase in service life [2]. Apart from residual stresses, SP also influences other parameters of the real structure. Using X-ray diffraction techniques, the impact of SP intensity on crystallite size, residual stresses, and texture were analysed. The depth distributions of these parameters in γ -Fe phase are described.

Three AISI 2205 rolled samples were used. One, which was not shot peened for reference, was labelled N, and two peened with pressure 1.5 bar and 7 bar were denoted P1.5 and P7, respectively. Rolling (RD), transversal (TD), and normal (ND) directions created their coordination system. The *Empyrean* and *X'Pert PRO MDP PANalytical* diffractometers with manganese and chromium X-ray tube were used. In order to obtain the depth distributions of above-mentioned parameters, the samples were gradually electrochemically polished.

The crystallite size was calculated using the Scherrer formula analysed by $\{211\}$ diffraction line. It was found that SP caused a reduction in crystallite size in subsurface layers. For example, crystallites were smaller for P1.5 sample by approximately 5 nm compared to sample N. With increasing distance from the sample surface, the crystallite

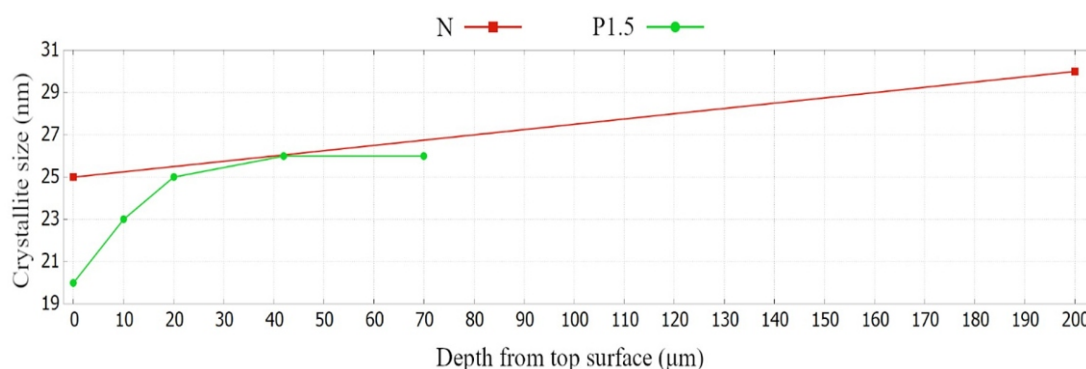


Figure 1. The depth distributions of the crystallite size of $\{211\}$ diffraction line for N and P1.5 samples

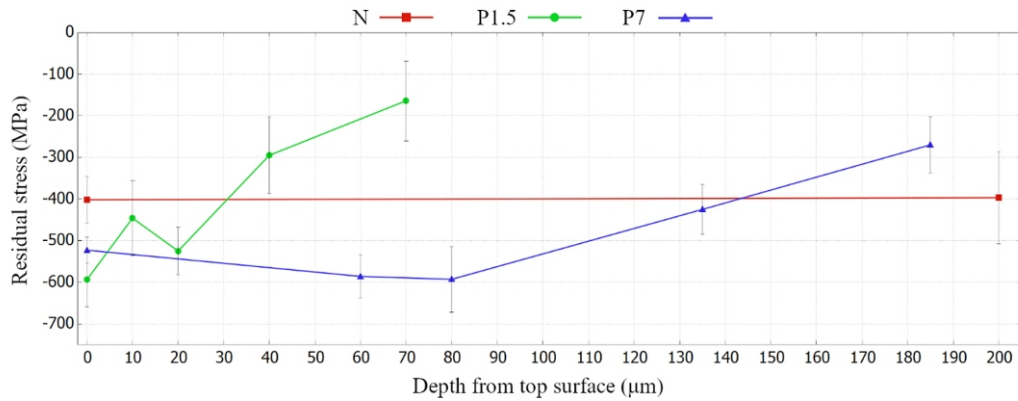


Figure 2. The depth distributions of the residual stresses in RD for all samples.

size changed to values comparable to those for sample N, as shown in Fig. 1.

The same diffraction line was used to analyse the residual stress distribution using “” method assuming the bi-axial state of the residual stresses with respect to RD and TD axis. As expected, SP led to an increase in compressive residual stresses in near-surface regions. Their surface values were around 600 MPa, 550 MPa, and 400 MPa (both directions) for P1.5, P7, and N, respectively. Similar to the case of crystallite size, the greatest change was also found near the surface. As the depth increased, the values decreased to stresses comparable to sample N. The depth distributions of the compressive residual stresses in RD are shown in Fig. 2.

The orientation distribution function (ODF) calculated from the experimental pole figures obtained by analysis of $\{110\}$, $\{200\}$, and $\{211\}$ diffraction lines was used for texture analysis. The MATLAB™ MTEX toolbox program [3] was used to calculate ODF. For N sample, the typical rolling texture of body-centred cubic materials was found. Crystallites were oriented along the incomplete α -fibre with a dominant $\{112\}\langle 110\rangle$ texture component in all measured depths. After SP, the texture components changed. They differed not only with respect to peening intensity but

also with respect to the distance from the surface for individual samples. Fig. 3 shows ODF in $\varphi_1 = 0^\circ$ sections for each sample on the surface. The texture components predominantly changed their significant planes. The $\langle 110\rangle$ direction remained preserved in most of the measured depths. It was also found that ODF are better described by particular texture components, rather than texture fibres.

1. TMR Stainless, Practical Guidelines for the Fabrication of Duplex Stainless Steel, London: IMO, 2014.
2. J. Champaine, Shot Peening Overview, *The Shot Peener*, 2001.
3. F. Bachman, R. Hielscher, H. Schaeben, Texture Analysis with MTEX – Free and Open Source Software Toolbox, *Solid State Phenomena*, **160**, (2010), 63-68.

This work was supported by the Grant Agency of the Czech Technical University in Prague, grant No. SGS22/183/OHK4/3T/14.

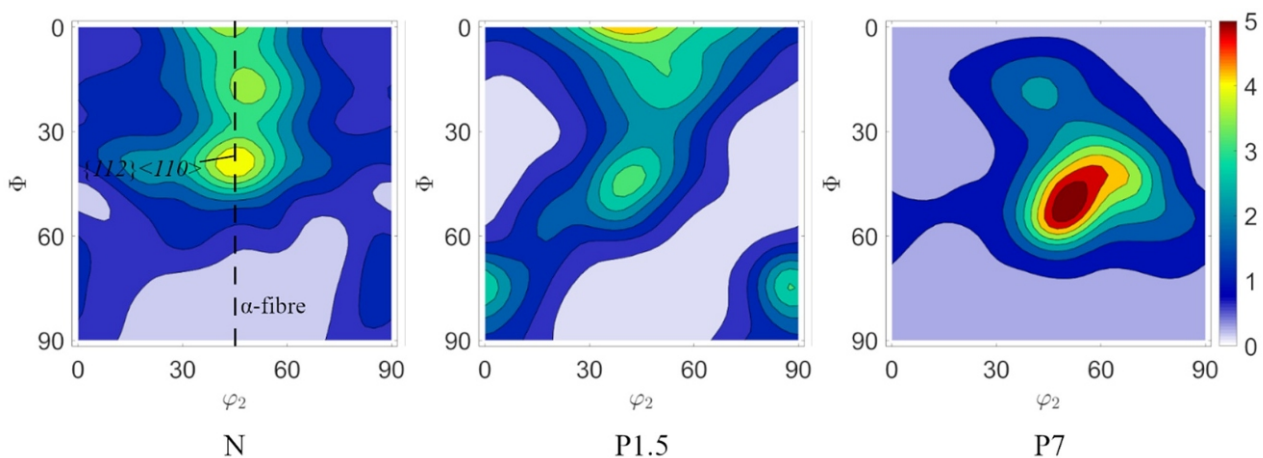


Figure 3. The ODF in $\varphi_1 = 0^\circ$ sections from surface for all samples. For sample N, α -fibre represented by dashed line and $\{112\}\langle 110\rangle$ texture component are shown.



SL9

IMPLEMENTATION OF GLOBAL OPTIMIZATION ALGORITHM PARTICLE SWARM OPTIMIZATION INTO PROGRAM FOX

Milan Kočí^{1,2}, Jan Drahokoupil^{1,2}

¹Faculty of Nuclear Science and Physical Engineering, Czech Technical University, Prague, Czech republic

²Institute of Physics of the Czech Academy of Science, Prague, Czech Republic

Determining crystal structures from powder diffraction patterns is a crucial technique in chemistry, physics, and materials engineering. The program FOX is one tool used for this purpose, and we extended the choice of optimizers by the particle swarm optimization (PSO) algorithm. Users can customize PSO parameters individually or use default settings. The algorithm can be interacted with through a graphical interface or via Python scripts. PSO was successfully applied to three crystal structures (PbSO₄, paracetamol, sofosbuvir), all of which were accurately identified

and matched published data. When compared to the parallel tempering algorithm, PSO produced better results in less time, particularly with the complex structure of sofosbuvir.

Kočí M. Implementace algoritmu optimalizace hejnem částic do programu FOX. (2024) Diploma theses. ČVUT, Praha.

In the program, this lecture was replaced by contribution by E. Spurná.

SL10

DIFFUSION DYNAMICS IN ECOLOGICAL CONCRETE STUDIED BY NEUTRON IMAGING METHOD

Jiří Zelenka

Czech Technical University in Prague, Faculty of Nuclear Sciences and Physical Engineering, Trojanova 13, Praha 2

Nowadays, most people in the world are experiencing the effects of climate change, so the goal of humanity is to achieve carbon neutrality. One of the main sources of CO₂ emissions is the energy and construction sectors. However, renewable sources do not provide enough to cover energy consumption in many regions. Nuclear power is one possible solution, but it generates nuclear waste that needs to be stored safely.

The aim of this study is to investigate the diffusion process of gadolinium nitride solutions in light and heavy water in a novel recycled concrete made of red brick rubble; the Gd³⁺ ions are used to mimic diffusion of actinides. Diffusion dynamics is studied by the neutron imaging method. Due to the sensitivity of our neutron camera imaging system, we are the first who report also on direct imaging of the diffusion of heavy water through the concrete matrix. For the solutions used, the diffusion coefficients and diffusion rates are calculated by using the second Fick's law. The obtained results are valuable in terms of the search for

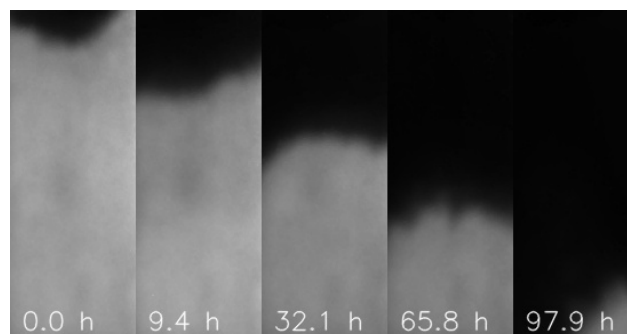


Figure 1. Neutron transmission images documenting the time evolution of diffusion, obtained for Sample 6. The actual diffusion time is shown.

a more sustainable and environmentally friendly option than conventional concrete in the construction of storage facilities for nuclear waste.

SL11

INSTRUMENT RESOLUTION FUNCTION OF 2D XRD SETUP AT THE P21.2 BEAMLINE AT PETRA III

R. Kaur^{1,2}, J. Bednarčík^{1,2}

Inst. of Physics, Fac. of Science, P.J. Šafárik Univ. in Košice, Park Angelinum 9, 04154 Košice, Slovakia
Institute of Experimental Physics, Slovak Academy of Science, Watsonova 45, 04001 Košice, Slovakia
ravneet.kaur@student.upjs.sk

The systematic study of reciprocal space resolution of two-dimensional X-ray diffraction (2D XRD) setup implemented at the P21.2 beamline is presented. Beam size, sample thickness and sample-to-detector distance were identified as key parameters, mostly affecting reciprocal space resolution. Few series of 2D XRD patterns were taken on powder LaB₆ standard sample with a monochromatic photon beam having energy of 81.84 keV. Beamsize (square profile) was set to four distinct sizes 0.1, 0.3, 0.5 and 1.0 mm. Sample thickness was set to 0.4, 1.0, 1.5 and 2.0 mm. Sample-to-detector distance was changed from 460 to 1800 mm. Scattered photons were acquired by 2D detector VAREX XRD4343CT (2880 x 2800 pixels, pixel size 150 μ m x 150 μ m, 16 bit intensity resolution). Altogether 144 patterns were acquired and used in analysis. Each 2D XRD pattern was azimuthally integrated, and its peak profiles were analyzed with pseudo-Voigt function. Instrument resolution function, i.e. variation of the peak full-width at half-maximum with Bragg angle 2θ was investigated as a function of the beam size, sample thickness and sample-to-detector distance.

Introduction

The Instrument resolution function (IRF) in X ray Diffraction (XRD) describes how the instrument itself influences the shape and width of the diffraction peaks. This function is crucial because it determines the inherent limitations of the instrument in terms of resolving power, affecting the accuracy and precision of the XRD measurements. The IRF is affected by several experimental parameters such as i) X ray source characteristics (degree of monochromaticity, source shape and size), ii) beam optics and collimation (beam divergence), iii) sample geometry (sample size, shape, alignment and positioning), iv) detector parameters (pixel size, detector distance from the sample), v) instrument geometry (goniometer precision, slit widths). All these imperfections and limitations associated with the real experimental setup contribute to the broadening of the experimentally observed diffraction profiles $I^{obs}(2\theta)$. The P21.2 beamline at PETRA III [1] is a high-performance beamline designed for a variety of advanced scientific experiments, particularly in the fields of material science, chemistry, and biology. Accurate determination of the instrument resolution function (IRF) is crucial for interpreting experimental data correctly. This study aims to characterize the IRF of the P21.2 beamline, providing insights into its performance and potential applications.

Research Methodology

To determine the IRF, we conducted a series of measurements using a combination of standard calibration LaB₆ sample [2] and advanced detection techniques. The methodology involved: 1) Performing a set of calibration measurements with the LaB₆ reference material using an experimental setup with a 2D detector on the P21.2 instrument of the PETRA III synchrotron source at DESY Hamburg. Calibration measurements were done with symmetrically varying parameters such as sample thickness, the photon beam cross section and the distance between the sample and 2D detector. 2) Analysis of acquired 2D diffraction patterns to characterize the angular resolution of the P21.2 instrument depending on the changing parameters. 3) Proposed a theoretical model based on the kinetic theory of diffraction and verification of its agreements with experimental data using a Monte Carlo simulation.

Results

The IRF curves shifted towards lower values with increasing SDD, independent of the sample thickness and beam size. For a given beam size and SDD, there is almost no variation of the IRF with the sample thickness. For a given sample thickness and SDD, the IRF shifts towards lower values with decreasing beam size. With decreasing beam size and sample thickness, the noise level in the IRF increases due to lower photon statistics and smaller scattering volume. Subsequently a simple theoretical model describing the single point scattering process based on kinematic theory of diffraction was proposed. Monte Carlo simulations of this model showed very good agreement with the experimental data. In spite the proposed model did not consider all the parameters that determine the angular resolution of the P21.2 instrument (e.g. divergence of the photon beam), the achieved agreement with the experimental results confirms the correctness of the assumptions of our model.

1. Schroer C.G., Wille H.C., Seek O.H., Bagschik K., Schulte-A Schrepping H., Tischer M., Graafsma H., Laasch W., Baev K., Klumpp S., Bartolini R., Reichert H., Leemans W. and Weckert The synchrotron radiations PETRA III and its future ultra-low-emittance-upgrade PETRA IV”, *The European Physical Journal Plus*, **137**(12), doi:10.1140/epjp/s13360-022-03517-6.
2. Black D., Windover D., Henins A., Filliben J. and Cline J., “Certification of Standard Reference Material 660b”, *Powder Diffraction*.
3. Benov D.M., “The Manhattan Project, the first electronic computer and the Monte Carlo method”, *Monte Carlo Methods and Applications*, **22**(1), (2016), 73–79, doi:10.1515/mcma-2016-0102.



SL12

ACCURATE STRUCTURE REFINEMENT FROM 3D ELECTRON DIFFRACTION DATA ON INORGANIC AND ORGANIC COMPOUNDS.

H. Chintakindi, S. Ashwin, L. Palatinus

*Department of Structure Analysis, Institute of Physics of Czech Academy of Sciences, Prague, Czechia
chintakindi@fzu.cz*

With the advent of 3D Electron diffraction (3D ED) techniques of data acquisition and processing, electron crystallography has emerged as a powerful technique for achieving accurate structure solutions and refinements at the atomic level [1]. In this study, we selected three samples two inorganic minerals, epidote and natrolite, and one organic, ibuprofen to address specific structural challenges. In both epidote and natrolite, the position of hydrogen atoms was difficult to determine due to the presence of heavier inorganic atoms. Epidote is a solid solution and has a mixed occupancy of Fe and Al in one site to be determined; natrolite being a non-centrosymmetric structure, necessitated the determination of its absolute orientation; ibuprofen is a beam sensitive organic sample that crystallizes in two different enantiomers. For ibuprofen we selected a sample that is enantiopure (S-form) to verify the accurate determination of the absolute structure.

All datasets were collected using a TEM FEI Tecnai G2 20 operating at an accelerating voltage of 200 kV and equipped with a Medipix 3 ASI Cheetah hybrid pixel detector. The data acquisition was performed through both precession-assisted stepwise 3D electron diffraction and continuous rotation 3D ED (Micro ED). Subsequent data processing was conducted using the PETS2 [2] software, and the structures were solved and refined using dynamical refinement in JANA2020 [3].

All three structures were successfully solved using dynamical refinement, allowing for the precise determination

of hydrogen atom positions. In the case of Epidote, the mixed occupancy of Fe and Al was accurately identified. Notably, the dynamical refinement of natrolite revealed a significant 10% difference in R-values between the two absolute orientations, highlighting a pronounced sensitivity to the left- and right-handed structures. For ibuprofen, due to its high beam sensitivity, a low dose cryo 3D ED experimental setup was essential to achieve successful structure resolution. The slight difference in R-values (1.27%) and the Z-score test were critical in determining the absolute configuration of S-ibuprofen, distinguishing it from R-ibuprofen.

1. Gemmi, M., Mugnaioli, E., Gorelik, T., Kolb, U., Palatinus, L., Boullay, P., Hovmöller, S. & Abrahams, J. (2019). *ACS Cent. Sci.* **5**, 1315–1329. P. J. Chupas, M. F. Ciraolo, J. C. Hanson, C. P. Grey, *J. Am. Chem. Soc.*, **123**, (2001), 1694.
2. Palatinus, L., Brázda, P., Jelínek, M., Hrdá, J., Steciuk, G., & Klementová, M. (2019). *Acta Cryst. B*, **75**, 512-522.
3. Petříček, V., Palatinus, L., Plášil, J., Dušek, M. (2023). *Z. Krist.*, **238**, 271-282.

This research was funded by the European Union's Horizon 2020 research and innovation programme under the Marie Skłodowska-Curie grant agreement No 956099 (NanED – Electron Nanocrystallography – H2020-MSCAITN).